

COLLISIONAL ORIGIN OF FAMILIES OF IRREGULAR SATELLITES

DAVID NESVORNÝ,¹ CRISTIAN BEAUGÉ,² AND LUKE DONES¹

Received 2003 October 9; accepted 2003 December 11

ABSTRACT

A distinctive feature of the irregular moons of the giant planets is their orbital grouping. Previously, the prograde and retrograde groups of irregular moons at Jupiter were believed to be groups of fragments produced by the disruption of two large moons. More recently, we have shown that the retrograde group has not one but probably four or more parent bodies. We also found that fragments were launched from two of the four identified parent moons, producing two clusters of irregular moons with members of each group having similar orbits. Named the Ananke and Carme families, these two groups consist of seven and nine known member moons, respectively. The origin of this orbital clustering is unknown. Current rates of collisions among satellites in the retrograde group are too low to explain them. Collisions with cometary impactors are even less likely. Groups of irregular satellites with similar inclinations at Saturn are also yet to be explained. It is conceivable that the satellite families are remnants from early epochs of solar system formation when impactors were more numerous. In this paper we investigate the possibility that satellite families formed via collisions between large parent moons and stray planetesimals. We find that the Ananke and Carme families at Jupiter could indeed have been produced by this mechanism, unless the residual disk of planetesimals in heliocentric orbit was already severely depleted when the irregular satellites formed. Conversely, we find that formation of the Himalia group of prograde Jovian satellites by the same mechanism is unlikely unless a massive residual planetesimal disk was still present when the progenitor moon of the Himalia group was captured. We place constraints on the mass of the residual disk (1) when satellites were captured, and (2) when the Ananke and Carme families formed. These values depend sensitively on the assumed size-frequency distribution of planetesimals.

Key words: planets and satellites: formation

1. INTRODUCTION

The irregular satellites of the Jovian planets are those moons that are far enough from their parent planet that the precession of their orbital plane is primarily controlled by the Sun (see Burns 1986). According to this definition, as of 2003 September 15, we know of 53 irregular satellites at Jupiter (Sheppard & Jewitt 2003), 14 at Saturn (Gladman et al. 2001a), six at Uranus (Gladman et al. 1998, 2000), and four at Neptune (Kuiper 1949; Holman et al. 2003).³

The irregular moons appear to show an interesting hierarchy of orbits. For example, Jupiter's irregular moons can be divided into two groups: seven prograde and 46 retrograde moons. The retrograde bodies, moreover, show two subgroups of tightly clustered orbits (the Carme and Ananke families; Nesvorný et al. 2003a; Sheppard & Jewitt 2003). These satellite groups are reminiscent of the distribution of orbits in the main asteroid belt, where disruptive collisions between asteroids produced groups of fragments sharing similar orbits (the so-called asteroid families; Hirayama 1918; Zappalà et al. 1994).

Using this analogy, we may ask whether disruptive collisions *between* irregular moons may explain their orbital

groupings. The answer is, probably not, or at least they cannot explain all the observed groups. Nesvorný et al. (2003a) calculated the rates of disruptive collisions between irregular moons. There it was found that approximately one collision per 1 Gyr occurs between known moons in the prograde group at Jupiter. Conversely, the retrograde group of Jovian irregular satellites has a much lower rate of collisions, because of the longer orbital periods of these moons and the large volume of space occupied by their orbits. The current impact rate on these moons from kilometer-sized comets and escaped Trojan asteroids is also negligible (Zahnle et al. 2003). It thus seems likely that the origin of the Carme and Ananke families (and also of some other groups of irregular moons; Nesvorný et al. 2003a) dates back to early epochs of the solar system, when impactors were more numerous.

To show that this scenario is plausible, we crudely estimate the number of disruptive collisions of irregular moons at Jupiter. We assume that a $100 M_{\oplus}$ residual planetesimal disk in the region of the Jovian planets, which we take to originally extend from 10 to 35 AU, contains $\sim 3 \times 10^{10}$ planetesimals with diameters ≥ 10 km and a 1 g cm^{-3} bulk density (§ 4). Beaugé, Roig, & Nesvorný (2002) estimated that a planetesimal has on average 27 encounters within 1 Hill radius of Jupiter before it is ejected from the solar system (see § 7). If the cumulative number of encounters within a distance R scales as R^2 , a 50 km radius moon of Jupiter (Himalia has a mean radius $R \sim 70$ km, Elara has $R \sim 35$ km) suffers $27(3 \times 10^{10}) \times [(50+5)/(5 \times 10^7)]^2 \approx 1$ disruptive collision. Here $R_H = 5 \times 10^7$ km is the Hill radius of Jupiter. Similar estimates yield about three collisions for Saturn's moon Phoebe, and about seven collisions for Neptune's moon Nereid. In these latter cases, however, impacts of 10 km diameter planetesimals on the moons are subcatastrophic, owing to the large sizes of

¹ Department of Space Studies, Southwest Research Institute, Suite 400, 1050 Walnut Street, Boulder, CO 80302.

² Observatorio Astronómico, Universidad Nacional de Córdoba, Laprida 854, X5000BGR Córdoba, Argentina.

³ See http://ssd.jpl.nasa.gov/sat_elem.html for an up-to-date list of orbital elements for all known planetary satellites; http://ssd.jpl.nasa.gov/sat_discovery.html lists the provisional and IAU-adopted names for the irregular satellites and lists the publications in which the discoveries were originally reported. Since these publications include more than 20 different IAU Circulars, we have not referenced them all here but refer the reader to the JPL Solar System Dynamics Web pages listed above. Note that our definition of irregular satellites excludes Neptune's large moon Triton and Saturn's moon Iapetus.

Phoebe and Nereid ($R \sim 110$ km and $R \sim 170$ km, respectively) and because the typical impact speeds are lower (§ 7). Nevertheless, collisions with external impactors may have been important for shaping the size and orbital distributions of smaller moons at these planets.

In this paper, we study the scenario in which the parent moons of satellite families were impacted by stray planetesimals. We show that the observed satellite families such as the Ananke and Carme groups (§ 2) may be outcomes of such events. We also determine the range of planetesimal disk masses that is compatible with the observed satellite families. To this end, we calculate the rates of collisions between bodies on elliptical and hyperbolic orbits (§ 3). To calculate the probability that a moon with a given orbit and diameter was disrupted or cratered during early stages, we generate the size-frequency distribution of planetesimal impactors (§ 4) and their orbital distribution (§ 5) and make use of standard scaling laws for impacts (§ 6). Results are presented in § 7.

2. OBSERVED SATELLITE FAMILIES

Historically, the distant satellites of Jupiter were believed to belong to two groups: the prograde group of irregular moons (including Himalia, Elara, Lysithea, and Leda) and the retrograde group (Pasiphae, Carme, Sinope, and Ananke). Researchers have struggled to explain these two groups by presuming that member moons of the two groups are fragments of two large, disrupted parent moons (Colombo & Franklin 1971; Pollack, Burns, & Tauber 1979). This basic presumption has been reexamined since the recent discoveries of the irregular moons at Jupiter.

To determine which satellites have similar orbits and may thus share a common origin, Nesvorný et al. (2003a) computed the mean orbital elements of irregular moons by averaging their orbital elements over 10^8 yr. These mean values are plotted in Figure 1 for the irregular moons of Jupiter.

The prograde group of irregular moons around Himalia (Themisto excluded; Figs. 1a and 1b) is more compact than the population of the retrograde moons (taken as a single group here; Figs. 1c and 1d). Assuming that these groups were formed by two collisional breakups (Colombo & Franklin 1971), we find that the collision that formed the prograde group was less energetic than the one that formed the retrograde group. We calculate from the Gauss equations⁴ that

$$\begin{aligned} \frac{\delta a}{a} &= \frac{2}{na(1-e^2)^{1/2}} [(1+e \cos f)\delta V_T + (e \sin f)\delta V_R], \\ \delta e &= \frac{(1-e^2)^{1/2}}{na} \left[\frac{e+2 \cos f + e \cos^2 f}{1+e \cos f} \delta V_T + (\sin f)\delta V_R \right], \\ \delta i &= \frac{(1-e^2)^{1/2}}{na} \frac{\cos(\omega+f)}{1+e \cos f} \delta V_W. \end{aligned}$$

Here a , e , and i are the semimajor axis, eccentricity, and orbital inclination of a satellite prior to an impact; δa , δe , and δi are the changes in these elements due to the impact; n is the orbital frequency of a satellite; and δV_T , δV_R , and δV_W are components of δV along the direction of the orbital motion, in the radial direction, and perpendicular to the orbital plane, respectively. Assuming that a satellite family originated by an impact, f and ω are the true anomaly and the perihelion argument of the parent body at the instant of the impact. If fragments are isotropically ejected from the breakup site with speeds V_{ejc} exceeding the escape velocity V_{esc} by $\delta V = (V_{\text{ejc}}^2 - V_{\text{esc}}^2)^{1/2} < V_{\text{max}}$, the Gauss equations show that their osculating orbital elements will be located within an ellipsoid centered at the parent body's initial (a , e , i) orbit. The size, shape, and orientation of the ellipsoid are determined by V_{max} , f , and ω .

$50 \text{ m s}^{-1} \lesssim \delta V \lesssim 400 \text{ m s}^{-1}$ for the prograde group, and $300 \text{ m s}^{-1} \lesssim \delta V \lesssim 500 \text{ m s}^{-1}$ for the retrograde group, where the δV is the ejection speed of individual fragments. Curiously, both these speed ranges (especially that for the population of the retrograde moons) are inconsistent with the velocity dispersion of multikilometer collisional fragments derived for catastrophic collisions by other means. For example, laboratory impact experiments, where centimeter-sized projectiles are shot into targets, and numerical hydrocode experiments, which are capable of simulating hypervelocity collisions among large bodies, both indicate that the mean and median ejection speeds from impacts are on the order of several times 10 m s^{-1} (Benz & Asphaug 1999; Michel et al. 2001). Similarly small ejection speeds were found for asteroid families that have not yet been dispersed by thermal forces (such as the Karin, Veritas, and Iannini families; Nesvorný et al. 2002, 2003b).

We are thus left with a contradiction: either we invoke some mechanism that further disperses orbits in addition to the velocity spread expected from their formation, or we should reject the scenario in which the prograde and retrograde populations of moons at Jupiter formed by collisional breakups of two precursor bodies.

A closer inspection of the retrograde satellite group shows that there exist several subclusters (Fig. 1; see also Nesvorný et al. 2003a; Sheppard & Jewitt 2003). The mean orbits of S/2000 J2, S/2000 J4, S/2000 J6, S/2000 J9, S/2000 J10, S/2001 J6, S/2001 J8, and S/2001 J11 cluster tightly around the mean orbit of J11 Carme, a ~ 46 km diameter moon; S/2000 J3, S/2000 J5, S/2000 J7, S/2001 J2, S/2001 J3, and S/2001 J7 have orbits similar to J12 Ananke, a ~ 28 km diameter moon. (The sizes quoted assume that Carme and Ananke have geometric albedos of 0.04; see Rettig, Walsh, & Consolmagno 2001.) Moreover, S/2000 J8 may be part of the group related to Pasiphae. Of the very recently discovered moons of Jupiter (not shown in Fig. 1), S/2003 J1, S/2003 J5, S/2003 J9, S/2003 J10, and S/2003 J11 may be members of the cluster around J11 Carme, and S/2003 J6 has an orbit similar to that of J12 Ananke.⁵

From the Gauss equations we find $5 \text{ m s}^{-1} \lesssim \delta V \lesssim 50 \text{ m s}^{-1}$ for the group of Carme (which we call the Carme family) and $15 \text{ m s}^{-1} \lesssim \delta V \lesssim 80 \text{ m s}^{-1}$ for the group of Ananke (the Ananke family). These speeds are more compatible with a δV expected from simple collisional breakups than the speeds computed for the whole population of retrograde moons.

Based on these results, Nesvorný et al. (2003a) proposed that the retrograde group of Jovian irregular moons witnessed a more complicated collisional history than thought before. In particular, it seems likely that we see fragments from at least two distinct precursor moons. The spectral differences between Carme and Ananke suggest that these precursor bodies correspond to two captured satellites rather than having a common ancestor (Luu 1991; Sykes et al. 2000; Brown 2000; Rettig et al. 2001; Grav et al. 2003). In a recent study, Grav et al. (2003) demonstrated that members of the Ananke and Carme families have homogeneous colors and suggested that they originated by fragmentation or cratering of two homogeneous progenitor moons.

Gladman et al. (2001a) classified the irregular moons of Saturn into groups of similar orbital inclination: the first satellite inclination group (S/2000 S4, S/2000 S10, and S/2000 S11),

⁵ These recently discovered moons do not have good orbital determinations yet, so their classification into groups is difficult.

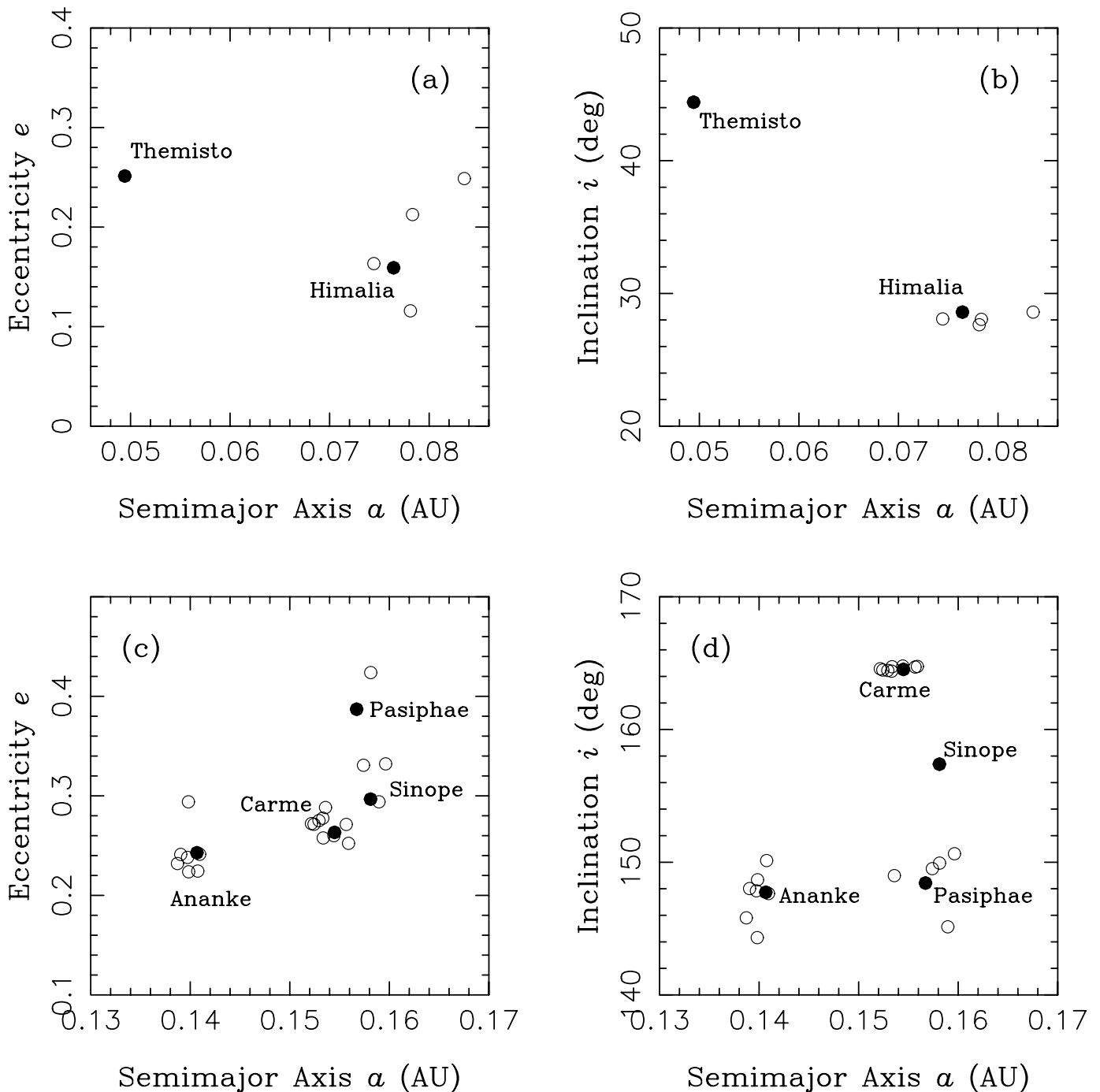


FIG. 1.—Orbits of the irregular satellites of Jupiter: (a, b) mean orbits of the prograde moons; (c, d) mean orbits of the retrograde moons. The mean orbital elements were taken from Nesvorný et al. (2003a). In (c) and (d), the orbits of many irregular moons are tightly clustered around the orbits of Ananke and Carme. The similarity of orbits of these moons suggests their common origin.

the second satellite inclination group (S/2000 S2, S/2000 S3, S/2000 S5, and S/2000 S6), and a rather loosely clustered Phoebe group (Phoebe, S/2000 S1, S/2000 S7, S/2000 S9, and S/2000 S12). The moons in each of these inclination groups probably do not have a common collisional origin, unless (1) asymmetric and large-magnitude ejection velocity fields occurred, or (2) collisions occurred early and some subsequent primordial mechanism modified the semimajor axes. Otherwise, it is hard to reconcile the magnitude and components of δV computed from the Gauss equations with the current understanding of collisional breakups (see Nesvorný

et al. 2003a or Grav et al. 2003 for a detailed discussion of this issue).

Because of the small number of Uranian and Neptunian irregular moons known at this moment, it is impossible to tell whether or not their orbits can be grouped in some way. Perhaps S/1997 U1 Caliban and S/1999 U2 Stephano may be linked (see Nesvorný et al. 2003a, their Fig. 13 and the related discussion, or Grav et al. 2003), but this association is yet to be demonstrated. In fact, the orbital distributions of Uranus's and Neptune's irregular moons are not statistically distinguishable from random distributions of orbits within stability limits.

Here we concentrate on the Ananke and Carme families at Jupiter because the δV -values determined for these two groups are compatible with impact-generated structures. If, indeed, the Ananke and Carme families were produced by collisions, we find that cratering impacts on Ananke and Carme can best explain them. To show this, we calculate the total volume of ejecta and compare it with the sizes of the parent moons. First we convert the magnitudes of the member moons into sizes assuming a geometric albedo $A = 0.04$ (Rettig et al. 2001). We then combine the volumes of the satellites within each group. We find that the total volumes of ejecta are $\sim 4.7 \times 10^{17}$ and $\sim 4.3 \times 10^{17}$ cm³ for the Ananke and Carme families, respectively. These volumes correspond to only 4% and 1% of the volumes of the parent moons, respectively. Using a 0.2 depth-to-diameter ratio (Schenk et al. 2004), we estimate that in both cases the crater diameters corresponding to these volumes are roughly 18 km. By comparison, Ananke and Carme are ~ 28 and ~ 46 km across. Thus, the putative family-forming impacts formed large craters on Ananke and Carme but did not catastrophically disrupt and disperse the parent moons.⁶

To relate the amount of ejecta to the impactor size, we use the scaling suggested by Schmidt & Housen (1987; see eq. [19] below). With a 1 g cm⁻³ density and a 1.25 km s⁻¹ impact speed (equal to the mean collision speed between the known retrograde irregular moons; see Nesvorný et al. 2003a), we find that a ~ 1.5 km diameter impactor is required in order to produce the Ananke family and that a ~ 1.65 km diameter impactor is required to produce the Carme family. With $N(>D) \sim 100[D/(1 \text{ km})]^{-2.5}$ (Sheppard & Jewitt 2003), where $N(>D)$ is the number of moons larger than diameter D , we find that $N(>1.5 \text{ km}) \approx 36$ and $N(>1.65 \text{ km}) \approx 29$. Nesvorný et al. (2003a) found that the probabilities of collision of Ananke and Carme with the other retrograde moons are 2.8×10^{-15} and 2.5×10^{-15} km⁻² yr⁻¹, respectively. Taken together, these numbers suggest cratering rates of 2×10^{-3} and 6×10^{-3} per impactor per 4.5 Gyr on Ananke and Carme, respectively.

With 36 and 29 impactors in the required size range and assuming Poisson statistics, we find only 7% and 15% probabilities that the Ananke and Carme families were produced by satellite-satellite collisions. We conclude that it is difficult to explain these satellite families by satellite-satellite collisions unless (1) more $D \gtrsim 1$ km moons exist than the number suggested by Sheppard & Jewitt (2003; these authors suggest that this number is known to within a factor of 2), or (2) the population of retrograde moons at Jupiter was much larger in the past. On the other hand, our estimate for the ejecta volume was conservative because we derived it from the observed, incomplete population of family members. Larger ejecta volumes and larger impactor sizes are probably more plausible. If so, it becomes even more difficult to explain the Ananke and Carme families by collisions *between* retrograde irregular moons.

We favor a scenario in which these satellite families were produced during early epochs of the solar system, when heliocentrically orbiting impactors were more numerous. To investigate this scenario in detail, we must (1) calculate collision rates between these impactors and moons, (2) model the

size-frequency and orbital distributions of impactors, and (3) use scaling laws to determine collision outcomes. Sections 3–6 address these issues.

3. COLLISION RATES BETWEEN MOONS AND PLANETESIMALS

To compute the rate of collisions between moons and planetesimals, we first recall that a population of satellites moving in Keplerian ellipses around planets with the same semimajor axis a , eccentricity $e < 1$, inclination i , and uniformly random λ , ϖ , and Ω has a space density distribution given by

$$P_1(r, \beta) = \frac{1}{2\pi^3 a^2 r} \frac{1}{\sqrt{e^2 - (r/a - 1)^2} \sqrt{\cos^2 \beta - \cos^2 i}} \quad (1)$$

(Kessler 1981; Nesvorný et al. 2003a) with the limits

$$a(1 - e) \leq r \leq a(1 + e), \quad -i \leq \beta \leq i. \quad (2)$$

Here $r = (x^2 + y^2 + z^2)^{1/2}$ and $\beta = \arcsin(z/r)$, where (x, y, z) are the Cartesian coordinates. The angular variables introduced prior to equation (1) are the mean longitude λ , longitude of pericenter ϖ , and longitude of the ascending node Ω . We normalized the above distribution to the total number of one body in the population, and thus $P_1(r, \beta) \Delta x \Delta y \Delta z$ is the probability that the body is located within an infinitesimal box $\Delta x \times \Delta y \times \Delta z$ centered at (x, y, z) .

Planetesimals that enter the Hill sphere of a planet generally move in hyperbolic orbits in a reference frame centered on the planet. Assuming a population of planetesimals with the same (planetocentric) a , $e > 1$, i , and uniformly random λ , ϖ , and Ω , the space density distribution of unbound orbits can be determined in a similar manner and yields

$$P_2(r, \beta) = \frac{K}{2\pi^3 a^2 r} \frac{1}{\sqrt{(r/a + 1)^2 - e^2} \sqrt{\cos^2 \beta - \cos^2 i}}. \quad (3)$$

Once we normalize the distribution in equation (3) to contain one body within a sphere of radius R , the constant K becomes

$$K = \pi \left\{ \sqrt{A^2 - e^2} - \ln \left[\frac{a}{e} \left(\sqrt{A^2 - e^2} + \frac{A}{a} \right) \right] \right\}^{-1}, \quad (4)$$

where $A = R/a + 1$.

Given these functions, the probability of collision per unit time between a body on an elliptical orbit with elements a_1 , e_1 , and i_1 and a body on a hyperbolic orbit with orbital elements a_2 , e_2 , and i_2 is

$$P_{\text{col}} = \pi(R_1 + R_2)^2 \times 2\pi \int_{r_{\min}}^{r_{\max}} \int_{\beta_{\min}}^{\beta_{\max}} P_1(r, \beta) P_2(r, \beta) V_{\text{col}}(r, \beta) \times r^2 \cos \beta dr d\beta, \quad (5)$$

where P_1 and P_2 are the probability distributions from equations (1) and (3) with (a_1, e_1, i_1) and (a_2, e_2, i_2) , respectively. The other quantities are defined as follows: the collision speed $V_{\text{col}} = |\mathbf{V}_1 - \mathbf{V}_2|$, where \mathbf{V}_1 and \mathbf{V}_2 are the orbital velocities of the two bodies; $r_{\min} = \max[a_1(1 - e_1), a_2(e_2 - 1)]$, $r_{\max} = \min[a_1(1 + e_1), R]$, $\beta_{\max} = \min[i_1, i_2, 180^\circ - i_1$,

⁶ We are severely underestimating the energetics of these family-forming impacts if (1) a large fraction of the ejected mass ended in small, unobserved fragments, or (2) many of the ejected fragments were destroyed by subsequent collisions (see § 8). While we believe that cratering impacts on Ananke and Carme are our best interpretation of the current observational data, the possibility that the Ananke and Carme families were produced by catastrophic breakups of much larger parent bodies cannot be ruled out.

$180^\circ - i_2]$, and $\beta_{\min} = -\beta_{\max}$; $\sigma = \pi(R_1 + R_2)^2$ is the effective cross section of the two bodies, with R_1 and R_2 being their effective radii [defined as $(3V_j/4\pi)^{1/3}$ for irregularly shaped bodies, where $V_j, j = 1, 2$, are their volumes].

The orbital velocities V_1 and V_2 at (x, y, z) are computed from (a_1, e_1, i_1) and (a_2, e_2, i_2) , respectively. Note that the collision probability in equation (5) is not a function of either $(\lambda_1, \varpi_1, \Omega_1)$ or $(\lambda_2, \varpi_2, \Omega_2)$, since these quantities are uniformly random variables (i.e., insofar as the space density distributions are given by eqs. [1] and [3]).

The integrals in equation (5) are not trivial, but they can be evaluated numerically with little difficulty.⁷ Using this new algorithm, we verified that our collision probabilities and speeds agree within 1% with values reported by Bottke & Greenberg (1993) and Manley, Migliorini, & Bailey (1998) for their test cases of asteroidal and cometary orbits. We also confirmed that our algorithm produces the expected result in a special case in which the moon's orbit is circular (Öpik 1951; Shoemaker & Wolfe 1982).⁸

4. SIZE-FREQUENCY DISTRIBUTION OF PLANETESIMALS

Let the differential and cumulative size-frequency distributions of heliocentric planetesimals be $N(d)$ and $N(>d)$, respectively, where d is the planetesimal's diameter.⁹ We use $N(d) = fN_{\text{EC}}(d)$, where $N_{\text{EC}}(d)$ is the differential size distribution of the present-day ecliptic comets (primarily derived from crater records on the Galilean satellites and Triton; Zahnle et al. 2003) and f is a multiplication factor. We will vary f over the range that gives plausible values for the total mass of the planetesimal disk (Hayashi, Nakazawa, & Nakagawa 1985).

It is notable that most small craters on Jupiter's moons appear to be secondaries, indicating a relative paucity of small impactors (Bierhaus et al. 2001; Bierhaus, Chapman, & Merline 2003; Schenk et al. 2004), while small craters on Triton imply a relatively abundant population of small impactors. However, it is unclear whether the craters on Triton are of heliocentric or planetocentric origin (Croft et al. 1995; Stern &

McKinnon 2000; Zahnle et al. 2001). We therefore, like Zahnle et al. (2003), present two cases, a case A, depleted in small impactors, in which the size-frequency distribution (SFD) is like that at Jupiter, and a case B in which small objects follow a distribution as at Triton. At large sizes, the SFD is constrained by observations of Kuiper belt objects: Gladman et al. (2001b) and Trujillo, Jewitt, & Luu (2001) found that $N(>d) \propto d^{-3.4}$ for $d > 50$ km and $N(>d) \propto d^{-3.0}$ for $d > 100$ km. We take the mean of the two power indices, that is, an index of -3.2 at large sizes.

Following Zahnle et al. (2003), our case A and B distributions are (here d is measured in kilometers)

$$N_A(>d) = N_{\text{cal}} \times \begin{cases} (d/1.5)^{-1}, & d < 1.5, \\ (d/1.5)^{-1.7}, & 1.5 \leq d < 5, \\ (1.5/5)^{1.7}(d/5)^{-2.5}, & 5 \leq d < 30, \\ (1.5/5)^{1.7}(5/30)^{2.5} \\ \quad \times (d/30)^{-3.2}, & d \geq 30; \end{cases} \quad (6)$$

$$N_B(>d) = N_{\text{cal}} \times \begin{cases} (d/1.5)^{-1.7}, & d < 1.5, \\ (d/1.5)^{-2.5}, & 1.5 \leq d < 30, \\ (1.5/30)^{2.5}(d/30)^{-3.2}, & d \geq 30. \end{cases} \quad (7)$$

We also consider, like Zahnle et al. (2003), as case C a distribution that is suggested by studies of the formation of Kuiper belt objects in situ (Stern 1995; Kenyon & Luu 1998; Kenyon 2002). This distribution assumes that the SFD of bodies with $d < 6.3$ km has Dohnanyi's (1972) equilibrium slope and the measured slope for Kuiper belt objects at larger sizes:

$$N_C(>d) = N_{\text{cal}} \times \begin{cases} (1.5/6.3)^{2.5}(d/6.3)^{-2.5}, & d < 6.3, \\ (1.5/6.3)^{3.2}(d/6.3)^{-3.2}, & d \geq 6.3. \end{cases} \quad (8)$$

In equations (6), (7), and (8), N_{cal} is a calibration constant defined as the number of planetesimals with $d > 1.5$ km. Assuming a 1 g cm^{-3} bulk density for a planetesimal, $N_{\text{cal}} = 1.5 \times 10^{12}$ gives a total mass of $100 M_{\oplus}$ for case A, $40 M_{\oplus}$ for case B, and $10 M_{\oplus}$ for case C. Hahn & Malhotra (1999) suggested that a disk mass on the order of $50 M_{\oplus}$ is required to expand Neptune's orbit by $\Delta a \sim 7$ AU, in order to explain the eccentricities of Pluto and its cohort of Kuiper belt objects at Neptune's 3:2 mean motion resonance. We will examine cases in which the residual planetesimal disk has a mass M_{disk} ranging from 10 to $200 M_{\oplus}$.

5. ORBITAL DISTRIBUTION FOR ENCOUNTERS

We analyzed the planetesimal encounters with the outer planets simulated by Beaugé et al. (2002) for the in situ formation of Uranus and Neptune and designed an "encounter generator," which is a fast code with several adjustable parameters [such as $N(D)$] that mimics the orbital distribution of encounters obtained in their realistic numerical integrations but is not limited to a small number of planetesimals. This was accomplished following a similar route as Zahnle, Dones, & Levison (1998) and Zahnle et al. (2001, 2003) in their studies of cratering rates on the regular satellites of the Jovian planets.

As expected, we found no preferred values in the distributions of the planetocentric angular variables ϖ (longitude of pericenter), Ω (longitude of node), and λ (mean longitude).

⁷ To avoid numerical problems for $r = a_1(1 \pm e_1)$, $r = a_2(e_2 - 1)$, $\beta = \pm i_1$, and $\beta = \pm i_2$, where the integrand has an integrable singularity, we use renormalization variables $t_1 = (r - q)^{1/2}$, $t_2 = (Q - r)1/2$, and $t_3 = (\cos^2 \beta - \cos^2 i)^{1/2}$.

⁸ Assuming a circular orbit for a moon, the impact probability per one planetesimal encounter is

$$P_1 = \frac{R_{\text{sat}}^2}{a_{\text{sat}}^2} \left(1 + \frac{v_{\text{esc}}^2}{v_{\text{orb}}^2 U^2} \right) \frac{U}{|U_x|} \frac{1}{\pi \sin i},$$

where R_{sat} is the satellite radius and v_{orb} and v_{esc} are the satellite's orbital speed and the escape velocity from its surface. U and U_x are the encounter speed and the radial component of the encounter velocity in units of the satellite's orbital speed v_{orb} (Öpik 1951). Following Öpik's formulae as written for hyperbolic orbits (Shoemaker & Wolfe 1982), we have

$$U^2 = 3 - (1 - e)/q - 2 \cos i \sqrt{q(1 + e)}, \\ U_x^2 = 2 - (1 - e)/q - q(1 + e), \\ v_i^2 = v_{\text{esc}}^2 + v_{\text{orb}}^2 U^2,$$

where q , e , and i are the planetocentric orbital elements of a stray planetesimal and v_i is the impact speed. Because $v_{\text{esc}} \ll v_{\text{orb}} U$ in our case, the effects of gravitational focusing in the above equations can be neglected.

⁹ Here and in the following we use d for the planetesimal's (i.e., impactor's) diameter to distinguish it from D , which we use for the moon's (i.e., target's) diameter.

We therefore assumed that these angles have uniform random values between zero and 2π . We found that the distribution of inclination i with respect to the planet's equator can be described by

$$N(<i) = \frac{1}{2}(1 - \cos i) \tag{9}$$

(see also Zahnle et al. 1998). This distribution corresponds to an isotropic distribution of velocities of planetesimals as seen by the planet.

Beaugé et al.'s (2002) simulations also yielded information about the distributions of planetocentric pericentric distances q of planetesimals. From their results we found that $N(<q) \propto q^2$ for $q > 0.06R_H$ and every outer planet. This is consistent with a regime in which high-speed hyperbolic encounters abound. For $q < 0.06R_H$, most of the encounters occur in quasi-parabolic orbits, and consequently, the square-law approximation ceases to be precise. This is not a problem, however, because we are primarily interested in the impact rates on irregular satellites, which are dominated by planetesimals with $q > 0.06R_H$.

5.1. Distribution of Jacobi Constant

In addition to ϖ , Ω , λ , i , and q , we need one last variable for the complete description of an encounter. Instead of the planetocentric eccentricity, we use the heliocentric Jacobi constant C because it provides an interesting link between local (planetocentric) variables and the global heliocentric distribution of the disk planetesimals. A detailed construction of the relationship between C and e is given in the Appendix. There we show that in planetocentric orbital elements, the Jacobi constant C is given by

$$C = c_0 + c_1 h + c_2 h^2, \tag{10}$$

where $h = [GM_0 q(1 + e)]^{1/2}$ is the planetocentric angular momentum per unit mass of the incoming body. The coefficients c_i are given by

$$\begin{aligned} c_0 = & \frac{2a_0 G(M_\odot + M_0)}{\sqrt{q^2 + a_0^2 + 2qa_0 \cos \theta}} - G(M_\odot + M_0) \\ & + 2GM_0 \left(\frac{a_0}{q} - 1 \right) + 2a_0 n_0 \sqrt{G(M_\odot + M_0) a_0} \\ & - 2a_0 \left(\frac{GM_0 q}{a_0^2} + a_0 n_0^2 q \right) \cos \theta, \end{aligned} \tag{11}$$

$$\begin{aligned} c_1 = & 2a_0 n_0 \cos i, \\ c_2 = & -a_0/q, \end{aligned} \tag{12}$$

where G is the gravitational constant, M_\odot and M_0 are the Sun's and the planet's masses, a_0 is the planet's semimajor axis, and n_0 is the planet's orbital frequency. Equation (10) with these coefficients is valid for any type of conic, be it elliptical ($e < 1$), parabolic ($e = 1$), or hyperbolic ($e > 1$). The coefficient c_0 depends on the phase angle θ ; the quantity $\pi - \theta$ gives the relative position of the pericenter with respect to the Sun in the planetocentric reference frame. We assume that θ is a random variable with a uniform distribution between zero and 2π .

We find that the distribution of C in Beaugé et al.'s (2002) numerical simulations bears a close resemblance to a lognormal distribution in $C_{\max} - C$, where C_{\max} is the maximum value of C detected for encounters with a given planet. We can

thus approximate the differential distribution of C via

$$\begin{aligned} N(C) = & \frac{1}{\sqrt{2\pi} |C_{\max} - C| S} \\ & \times \exp \left\{ -\frac{[\log(C_{\max} - C) - M]^2}{2S^2} \right\}, \end{aligned} \tag{13}$$

where M and S are the mean value and standard deviation, respectively. These parameters were determined numerically from Beaugé et al.'s data (Table 1).

A comparison between the determined lognormal distributions of C and the distributions of C obtained numerically by Beaugé et al. (2002) is shown in Figure 2. The numerical distribution for Jupiter shows some peaks and valleys that are not reproduced by the lognormal distribution. In addition, the lognormal distribution shows somewhat larger values at $C \sim 2.9-3.0$ than the numerical data. The errors introduced by this compromise are small in the context of this work.

The cumulative distribution for a lognormal function is given by

$$N(>C) = \frac{1}{2} + \frac{1}{2} \operatorname{erf} \left[\frac{\log(C_{\max} - C) - M}{\sqrt{2}S} \right], \tag{14}$$

where erf is the error function. Taking $x = N(>C)$ with $x \in [0, 1]$ and inverting equation (14), we obtain

$$\log(C_{\max} - C) = M + \sqrt{2}S \operatorname{erf}^{-1}(2x - 1). \tag{15}$$

Thus, in terms of a uniform random variable $x \in [0, 1]$, the distribution of C is given by

$$C = C_{\max} - \exp[M + \sqrt{2}S \operatorname{erf}^{-1}(2x - 1)]. \tag{16}$$

5.2. Distribution of Eccentricities

So far, and apart from the trivial angular variables, we obtained the encounter distributions in terms of C , q , and i . Inverting equation (10), we determine the angular momentum as $h = h(C, q, i, \theta)$, where θ is a random angle. Finally, using the relationship between angular momentum and eccentricity, we get

$$e = \frac{h^2}{qGM_p} - 1. \tag{17}$$

Figure 3 shows the eccentricity distributions for Jupiter and Neptune for $q = 0.2R_H$, $0.4R_H$, and $0.8R_H$. The agreement between model and numerical distributions is good. In general, the model distribution reproduces the numerical data with

TABLE 1
PARAMETERS OF THE LOGNORMAL DISTRIBUTION OF THE JACOBI CONSTANT FOR EACH PLANET

Planet	C_{\max}	M	S
Jupiter.....	3.039	-1.694	0.780
Saturn.....	3.017	-1.856	0.928
Uranus.....	3.005	-2.750	1.315
Neptune.....	3.006	-2.773	1.311

NOTES.—The columns list the maximum value of C detected for encounters with a given planet (C_{\max}), the mean value of C (M), and the standard deviation of C (S). These parameters are used by our encounter-generator program to produce distributions of C .

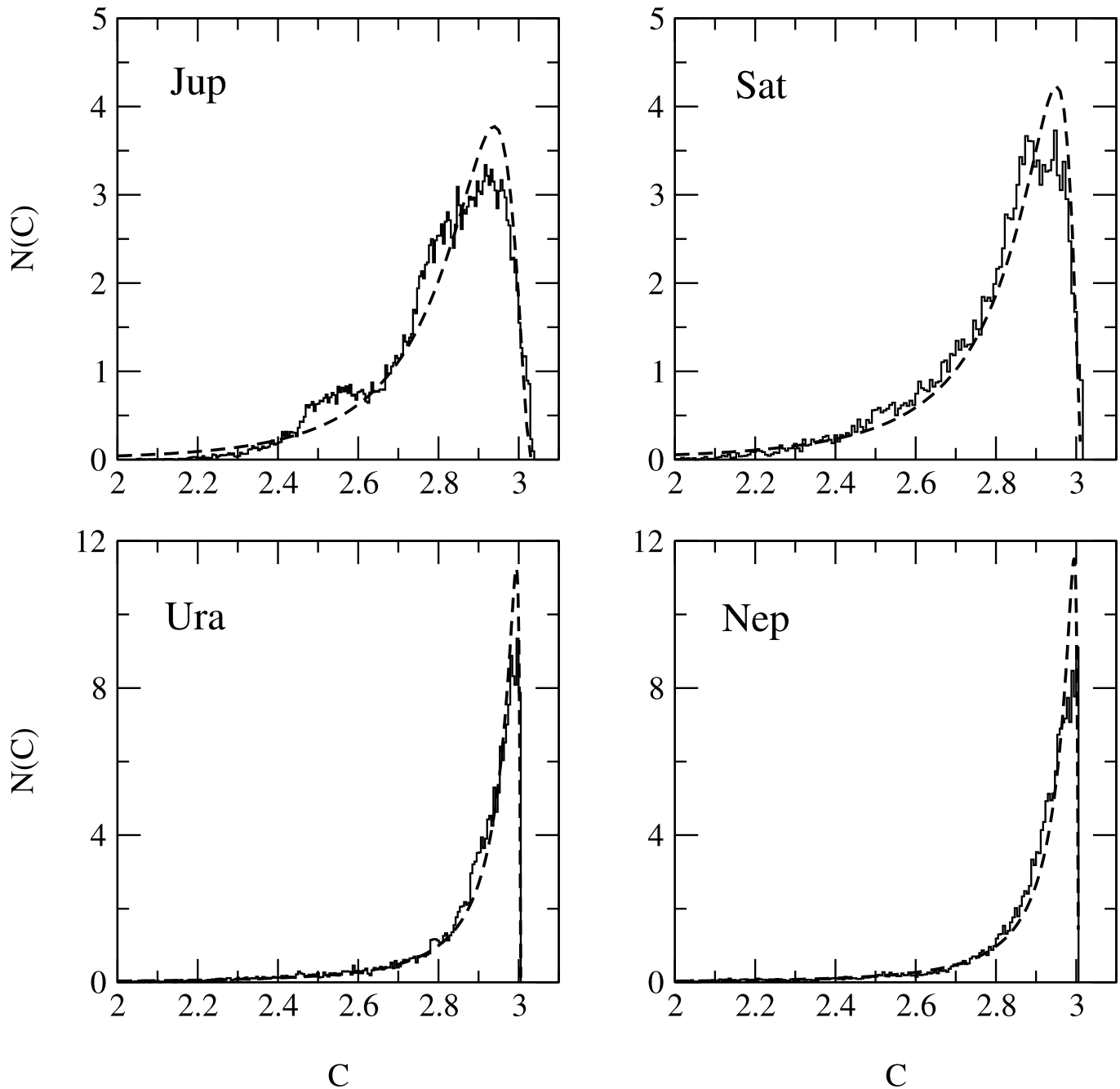


FIG. 2.—Differential distributions of the Jacobi constant from Beaugé et al. (2002, *solid lines*) and our lognormal fits (*dashed lines*; eq. [13]). Parameters of the lognormal distribution are given in Table 1.

errors smaller than $\sim 20\%$ for $q \gtrsim 0.1R_H$. Errors of this order will not affect our results, because uncertainties in other model parameters (e.g., the SFD of planetesimals) are much larger. For $q \ll 0.1R_H$ (not shown here), the model distribution is deficient in quasi-parabolic orbits (i.e., orbits with $e \sim 1$). Fortunately, these values of q are less relevant for this study because encounters at small q are infrequent. Consequently, most impacts on the irregular moons occur from impactors with $q \gtrsim 0.1R_H$.

6. SCALING FOR IMPACTS

We will study two cases: (1) impacts that lead to catastrophic disruptions of moons and dispersal of the resulting fragments, and (2) large cratering impacts. While case 1 is

important to understand issues related to satellite survival, case 2 is more relevant for satellite families at Jupiter.

For case 1, we use the threshold for a catastrophic disruption and dispersal of fragments determined by Benz & Asphaug (1999). They used a smoothed particle hydrodynamics method to simulate colliding rocky and icy bodies in an effort to self-consistently define the threshold Q_D^* . This threshold is defined as the specific energy required to shatter the target body and disperse the fragments into individual but possibly reaccumulated objects, the largest one having exactly half the mass of the original target. Where appropriate, we will use a simplified terminology in the following text, where by catastrophic “disruption” we mean catastrophic disruption of the parent body *and* dispersal of the resulting fragments

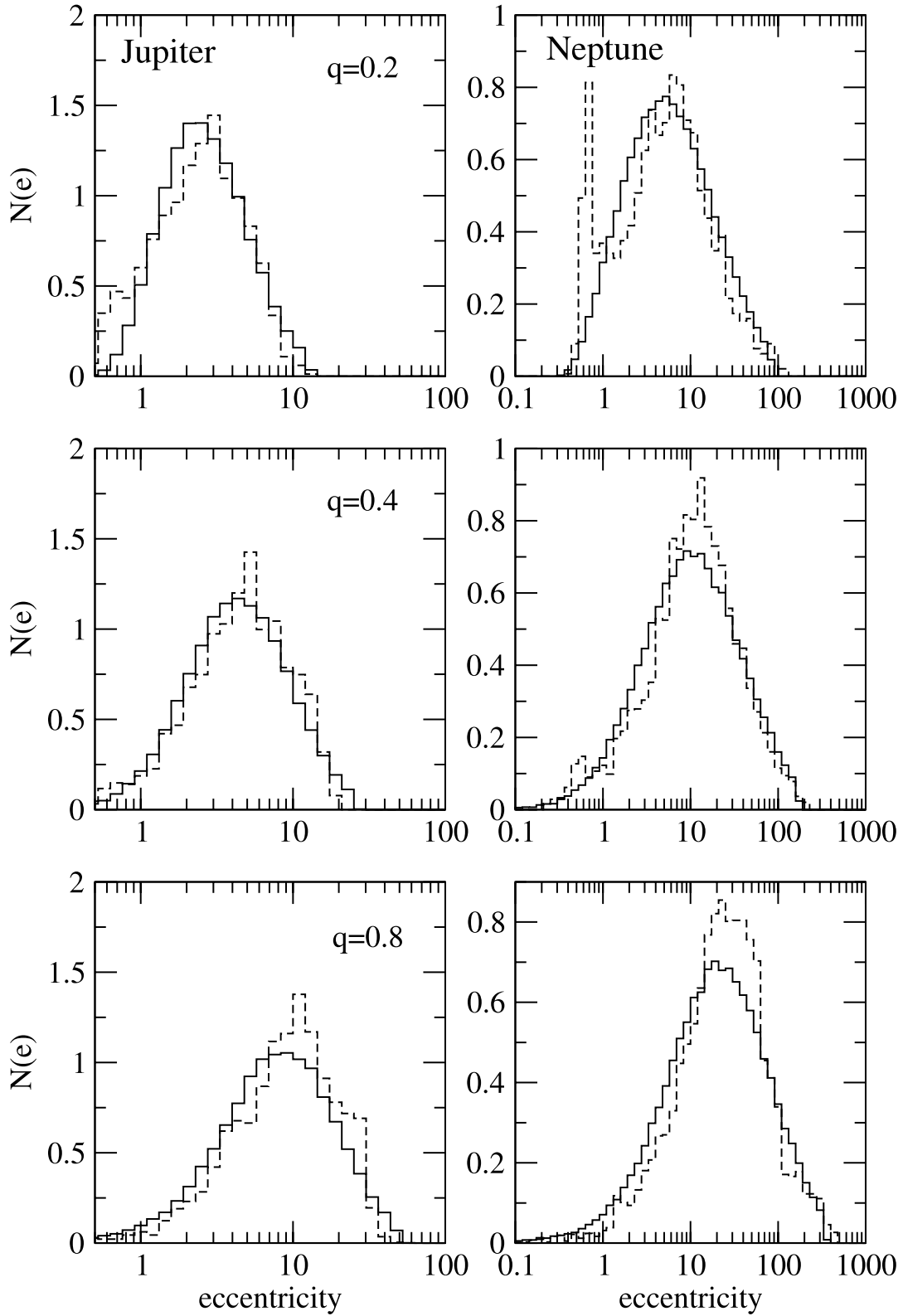


FIG. 3.—Comparison between model and numerical distribution of eccentricities for Jupiter (*left*) and Neptune (*right*) for $q = 0.2R_H$, $0.4R_H$, and $0.8R_H$. Histograms in dashed lines show numerical data obtained from Beaugé et al. (2002); histograms in solid lines are the model distributions (see eq. [16]). The peak present for Neptune at $q = 0.2R_H$ is probably caused by the temporary capture of one or a few planetesimals and is thus beyond the scope of our model.

in the sense defined above. We will not study cases in which precursor moons were catastrophically disrupted but not dispersed (i.e., shattered; see Richardson et al. 2002 for a definition), because these events do not produce observable families.

The functional form of Benz & Asphaug's (1999) law is given by

$$Q_D^* = Q_0(R_{PB})^a + B\rho(R_{PB})^b \text{ ergs g}^{-1}, \quad (18)$$

where R_{PB} is the radius of the parent body (in centimeters), ρ is the density of the parent body (in g cm^{-3}), and Q_0 , B , a , and b are constants. This functional form represents two distinct regimes, dominated by (1) material strength (first term, $a < 0$) and (2) self-gravity (second term, $b > 0$). Because self-gravity dominates for $R_{PB} \gtrsim 100\text{--}200$ m (Benz & Asphaug 1999), we concentrate on the second term in equation (18).

We will assume that irregular moons are primarily composed of ice. Benz & Asphaug (1999) calculate coefficients B and b for ice and two different impact speeds: 0.5 and 3 km s^{-1} . For 0.5 km s^{-1} , $B = 2.1 \text{ ergs cm}^3 \text{ g}^{-2}$ and $b = 1.19$. For 3 km s^{-1} , $B = 1.2 \text{ ergs cm}^3 \text{ g}^{-2}$ and $b = 1.26$. Because impact speeds (V_{imp}) between planetesimals and satellites range between 0.5 and 10 km s^{-1} (Beaugé et al. 2002; Table 2 of this paper), we interpolate/extrapolate from the B and b given by Benz & Asphaug to obtain Q_D^* for any value of the impact speed.

For cratering impacts, we use the scaling law derived from laboratory experiments of impacts into sand and from large explosions. Schmidt & Housen (1987; supplemented with the angular dependence assumed by Zahnle et al. 2003) suggest the following relation for the volume of a crater:

$$V = 0.13 \left(\frac{m_i}{\rho_t} \right)^{0.783} g^{-0.65} \left(\frac{\rho_i}{\rho_t} \right)^{0.217} v_i^{1.3} \cos \alpha \text{ cm}^3, \quad (19)$$

where the impactor has mass m_i , density ρ_i , and speed v_i , and where the surface gravity is g and the target density is ρ_t . All quantities in equation (19) have to be evaluated in cgs units. The incidence angle α is measured from the zenith. The mean and median value for the incidence angle for isotropic velocities is 45° . We will assume $\alpha = 45^\circ$.

Strictly speaking, equation (19) applies only to the volume of a geometrically simple, bowl-shaped transient crater that forms immediately after impact; a different scaling applies to larger, morphologically complex craters (Zahnle et al. 2003). We use equation (19) for the following reasons: (1) Craters on the Moon that have diameters smaller than about 15 km are simple craters. The transition from simple to complex should occur at a smaller crater size for a lunar-sized body made of a weaker material, such as ice. However, the size above which a crater is complex is expected to be larger for a smaller body (because gravity is weaker). When the competing effects of material strength and gravity are taken into account, it appears likely that complex craters may not occur at all on most irregular satellites. (2) Even if we used the relation given by Zahnle et al. (2003) for icy satellites (see Schenk et al. 2004), complex craters would be at most 50% bigger in diameter than simple craters. That accuracy is adequate for us because the uncertainty originating from the Schmidt & Housen (1987) scaling relationship is probably of comparable size. Moreover, volumes of simple (eq. [19]) and complex (Zahnle et al. 2003) craters differ by less than 50% , because complex craters are shallower than the simple craters.

7. RESULTS

We calculate the rates of disruptive and cratering collisions of real and fictitious irregular moons. For each real irregular moon, we assume that its orbital elements a , e , and i are fixed and equal to the mean values determined by Nesvorný et al. (2003a). We neglect gravitational focusing by the moons, which is negligible in the regime of sizes and impact speeds investigated here.

Table 2 shows the mean collision probabilities per encounter per area ($\pi P_{\text{col}}/\sigma$) and mean impact speeds (V_{col}) for selected irregular moons.¹⁰ For Jupiter, we list only the largest moons of every group. The quantities P_{col} and V_{col} were computed by averaging over 10^5 planetesimal encounters within 1 Hill radius of a planet. This number of encounters is large enough to attain the convergence limit to within a 1% precision. The encounters were generated using the recipe explained in § 5.

In Table 2, the collision speeds V_{col} are generally larger for moons that are closer to a planet. This is expected because the orbital speeds of satellites and planetocentric speeds of planetesimals are both larger at smaller distances from the planet (Beaugé et al. 2002). Also, the collision probabilities P_{col} are larger at smaller distances. What we see here is probably the effect of gravitational focusing by the parent planet. In the absence of gravitational focusing, P_{col} would be roughly constant with planetocentric distance because all locations within a Hill sphere would be receiving roughly the same number of planetesimals. In fact, the difference in P_{col} between the innermost and outermost irregular satellites of a given planet is not large. The effects of gravitational focusing by a planet are more important for the regular moons that orbit at smaller a than for the irregular satellites (Zahnle et al. 2003).

Because P_{col} and V_{col} do not vary much among the irregular moons of planet j ($j = 5\text{--}8$ from Jupiter to Neptune), we calculate their mean values $\langle P_{\text{col}} \rangle_j$ and $\langle V_{\text{col}} \rangle_j$ (Table 2) and use $\langle P_{\text{col}} \rangle_j$ and $\langle V_{\text{col}} \rangle_j$ to discuss the disruption and cratering rates on the irregular moons of planet j . The mean values $\langle P_{\text{col}} \rangle_j$ and $\langle V_{\text{col}} \rangle_j$ progressively decrease with the increasing semimajor axis of a planet, that is, from Jupiter to Neptune. For this reason, we expect that the consequences of planetesimal bombardment were more severe at Jupiter than at Neptune. At first glance, this result may be compatible with observations, because the orbital distribution of Jovian irregular satellites shows clear signatures of past collisions (e.g., the Ananke and Carme families), while the same structures are not observed among the irregular satellites of Saturn, Uranus, and Neptune. Unfortunately, we do not yet know of enough irregular moons with $1\text{--}10 \text{ km}$ diameters at Saturn, Uranus, and Neptune to detect structures like the Ananke and Carme families at these planets. Moons of these sizes at Saturn, Uranus, and Neptune are very faint and difficult to detect (see, e.g., Nesvorný & Dones 2002).

We use the following procedure to calculate the probability that a diameter D moon of planet j is catastrophically disrupted: For Q_D^* (eq. [18]) and the characteristic impact speed $\langle V_{\text{col}} \rangle_j$ (Table 2), we calculate the diameter d^* of the smallest impactor that can catastrophically disrupt the moon. The total population of impactors larger than this size is $N(>d^*)$ (eqs. [6]–[8]). Beaugé et al. (2002) found that every planetesimal suffers on average $N_j^{\text{enc}} = 27.4, 21.4, 31.9$, and

¹⁰ The quantity listed as $10^{14}P_{\text{col}}/\sigma$ in Tables 5, 6, and 7 of Nesvorný et al. (2003a) should have been labeled $10^{14}\pi P_{\text{col}}/\sigma$. The calculations of impact rates in Nesvorný et al. (2003a) are correct.

TABLE 2
COLLISION RATES AND IMPACT SPEEDS FOR IRREGULAR SATELLITES

Satellite	$\pi P_{\text{col}}/\sigma$ (10^{-16} km^{-2})	$\langle V_{\text{col}} \rangle$ (km s^{-1})	$\langle a \rangle$ (AU)	$\langle e \rangle$	$\langle i \rangle$ (deg)	D (km)
Jupiter:						
Themisto (S/1975 J1)	4.24	8.70	0.049422	0.2513	44.41	8
Leda	4.12	7.78	0.074448	0.1633	28.07	20
Himalia	4.12	7.73	0.076427	0.1591	28.59	120×150
Elara	4.10	7.65	0.078113	0.1158	27.63	86
Lysithea	4.10	7.70	0.078334	0.2126	28.05	36
Ananke	3.80	6.70	0.14067	0.2429	147.73	28
Carme	3.79	6.58	0.15450	0.2633	164.53	46
Pasiphae	3.77	6.50	0.15671	0.3871	148.43	60
Sinope	3.77	6.52	0.15811	0.2967	157.39	38
Average	3.99	7.32				
Saturn:						
Kiviuq (S/2000 S5)	3.32	5.11	0.075561	0.3082	47.90	17
Ijiraq (S/2000 S6)	3.32	5.10	0.075914	0.3027	48.00	14
Phoebe	3.31	5.07	0.086478	0.1642	175.18	240
Paaliaq (S/2000 S2)	3.24	4.87	0.10035	0.3462	49.23	25
Skadi (S/2000 S8)	3.22	4.88	0.10412	0.2731	152.00	8
Siarnaq (S/2000 S3)	3.21	4.78	0.11739	0.3180	47.73	45
Erriapo (S/2000 S10)	3.21	4.74	0.11706	0.4690	37.49	10
Albiorix (S/2000 S11)	3.22	4.79	0.10949	0.4907	37.46	30
Tarvos (S/2000 S4)	3.21	4.77	0.12126	0.5178	38.07	16
Mundilfari (S/2000 S9)	3.20	4.76	0.12421	0.2079	167.14	7
Suttung (S/2000 S12)	3.18	4.67	0.12938	0.1155	176.05	7
Thrym (S/2000 S7)	3.18	4.69	0.13553	0.4709	175.56	7
Ymir (S/2000 S1)	3.14	4.63	0.15334	0.3368	173.06	20
Average	3.23	4.84				
Uranus:						
Caliban (S/1997 U1)	3.37	2.70	0.047900	0.1922	141.19	60
Stephano (S/1999 U2)	3.34	2.65	0.053133	0.2325	143.46	20
Sycorax (S/1997 U2)	3.23	2.44	0.081501	0.5197	156.93	120
Prospero (S/1999 U3)	3.19	2.38	0.10952	0.4378	149.32	30
Setebos (S/1999 U1)	3.16	2.36	0.11711	0.5776	153.58	30
Average	3.26	2.51				
Neptune:						
Nereid	1.57	2.46	0.03690	0.7460	9.66	340
Average	1.57	2.46				

NOTES.—The columns are satellite name, “intrinsic” collision probability ($\pi P_{\text{col}}/\sigma$, from eq. [5]), mean collision speed (V_{col}), mean semimajor axis ($\langle a \rangle$), mean eccentricity ($\langle e \rangle$), mean inclination ($\langle i \rangle$), and diameter (D). The intrinsic collision probability is given in units of 10^{-16} km^{-2} per encounter of a planetesimal within $1R_{\text{H}}$ of a planet. Mean orbital elements were taken from Nesvorný et al. 2003a. The sizes of most moons were calculated from their magnitudes using albedos $A = 0.04, 0.05,$ and 0.07 for satellites of Jupiter, Saturn, and Uranus, respectively. The sizes for Himalia and Nereid were taken from Porco et al. 2003 and Thomas, Veverka, & Helfenstein 1991.

51.2 encounters within 1 Hill radius of Jupiter, Saturn, Uranus, and Neptune, respectively, before it is removed from the solar system. The disruption rate is then $x = N_j^{\text{enc}} N(>d^*) \langle \pi P_{\text{col}}/\sigma \rangle_j \times (D/2)^2$, where $\langle P_{\text{col}} \rangle_j$ is taken from Table 2. The probability $p(D)$ that the diameter D moon is catastrophically disrupted by impacts from the residual planetesimal disk of mass M_{disk} is $p(D) = 1 - \exp(-x)$ (according to Poisson statistics), where M_{disk} is calculated from equations (6), (7), and (8) using a bulk density of 1 g cm^{-3} for planetesimals.

Figures 4, 5, and 6 show $p(D)$ for our case A, B, and C size-frequency distributions of planetesimals, respectively. We first discuss these cases separately.

Figure 4 shows an interesting behavior of $p(D)$. Large moons ($D > 100 \text{ km}$) are difficult to disrupt because a large d^* is needed and there are not enough impactors with diameters greater than d^* for plausible values of M_{disk} . On the other hand, $p(D)$ decreases with D for $D < 10 \text{ km}$ because $N_A(>d)$ is very shallow for $d < 1 \text{ km}$ and there are just not enough impactors in this size range to compensate for the small cross

sections of $D < 10 \text{ km}$ moons. In effect, planetesimals with our case A size-frequency distribution $N_A(>d)$ will preferentially disrupt satellites of intermediate sizes ($D \sim 10$ – 100 km).

Figure 5 tells a different story. Because $N_B(>d)$ is steeper than $N_A(>d)$ at small d , there are now enough small impactors to make the survival of small moons difficult. The transition from high to low probability of disruption generally occurs in the 10–100 km diameter range. The same transition is more abrupt in case C because $N_C(>d)$ (eq. [8]) is steeper than $N_B(>d)$ down to smaller sizes (Fig. 6). With $N_C(>d)$, satellites with $D \lesssim 10 \text{ km}$ have disruption probabilities of ~ 1 for even the smallest considered M_{disk} ($=10 M_{\oplus}$). This makes the survival of early-captured $D \lesssim 10 \text{ km}$ moons difficult.

8. DISCUSSION

To place Figures 4–6 in the context of satellite formation, we describe the likely sequence of events that led to the capture of irregular satellites. The irregular satellites were

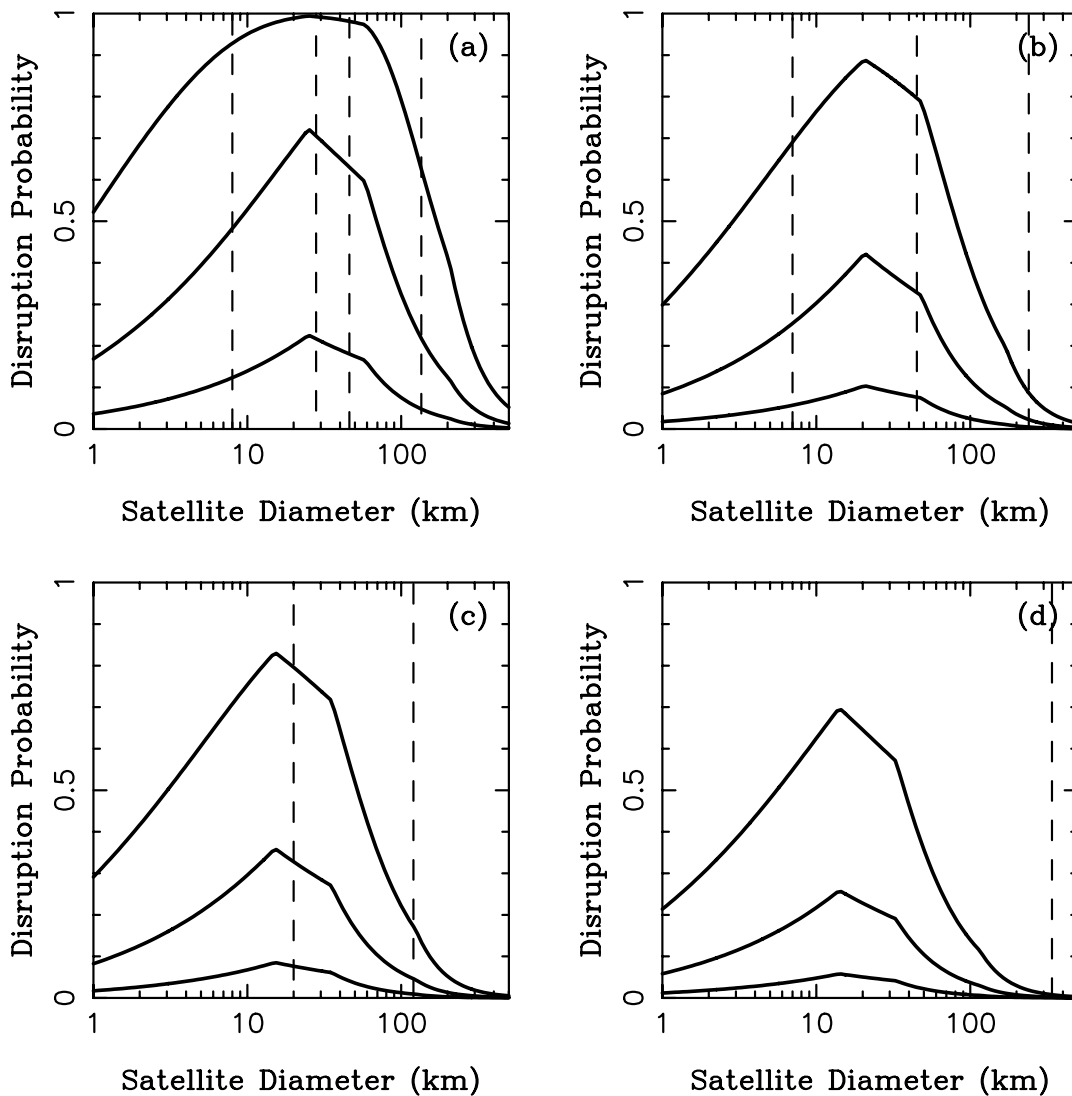


FIG. 4.—Disruption probability $p(D)$ of irregular satellites from impacts by stray planetesimals: (a) Jupiter, (b) Saturn, (c) Uranus, and (d) Neptune. The planets gradually eliminate the residual planetesimal disk at 10–35 AU and send numerous potential impactors into planet-crossing orbits. For impactors, we use $N_A(>d)$ (eq. [6]) normalized to $M_{\text{disk}} = 10, 50,$ and $200 M_{\oplus}$ (solid lines; from bottom to top). The sizes of selected irregular satellites are denoted by vertical dashed lines. Survival of these moons is likely only for low $p(D)$. From left to right, we show (a) Themisto, Ananke, Carme, and Himalia at Jupiter; (b) the smallest known irregular moons, S/2000 S3 (Siarnaq) and Phoebe at Saturn; (c) Stephano and Sycorax at Uranus; and (d) Nereid at Neptune.

probably captured via dissipation of their orbital energy in circumplanetary gas disks (Pollack et al. 1979; Čuk & Burns 2004). Indeed, an object that suffers a low-speed encounter with a planet may be temporarily captured even in the absence of a disk (Kary & Dones 1996), then lose kinetic energy via aerodynamic drag in the residual circumplanetary gas disk, and eventually end up on a planet-bound orbit. These events probably occurred during the late phases of the circumplanetary disk’s lifetime, because otherwise the captured object would spiral into the planet by the effects of gas drag (Pollack et al. 1979; Čuk & Burns 2004). By contrast, in the late stages of formation of the Jovian planets, the surface density in the circumplanetary disk was likely orders of magnitude smaller than in a “minimum mass” nebula, and the lifetime against gas drag, even for a kilometer-sized irregular satellite, probably exceeded 1 Myr (Canup & Ward 2002; Mosqueira & Estrada 2003a, 2003b).

During early epochs, satellites must have survived not only the effects of circumplanetary gas drag, but also a phase of heavy bombardment during which myriads of planetesimals

were traversing the planets’ neighborhoods. To constrain the maximum mass of the planetesimal disk at the time of the irregular moons’ formation, we will require that the collision rates between moons and planetesimals were low enough to guarantee the moons’ survival. We will use Figures 4, 5, and 6 to this end. It is also clear that the mass in the planetesimal disk was not strongly depleted when the irregular moons formed if the irregular moons are, in fact, captured planetesimals.

For the case B and C distributions (Figs. 5 and 6), survival of an irregular satellite at Jupiter was unlikely unless (1) the moon was large enough or (2) the planetesimal disk was already partially depleted when the moon was captured. For example, the probability of catastrophic disruption $p(D) < 0.5$ for case C for $D \gtrsim 60$ km and $M_{\text{disk}} = 10 M_{\oplus}$ and for $D \gtrsim 80$ km and $M_{\text{disk}} = 50 M_{\oplus}$. Because parent retrograde irregular satellites at Jupiter have $28 \text{ km} \lesssim D \lesssim 60 \text{ km}$, we require $M_{\text{disk}} \lesssim 10 M_{\oplus}$ for their survival if case C applies. Most prograde irregular satellites at Jupiter probably derive from a single large parent body with $D \sim 150$ km (Čuk & Burns 2004). Interestingly, the breakup of this large parent moon by

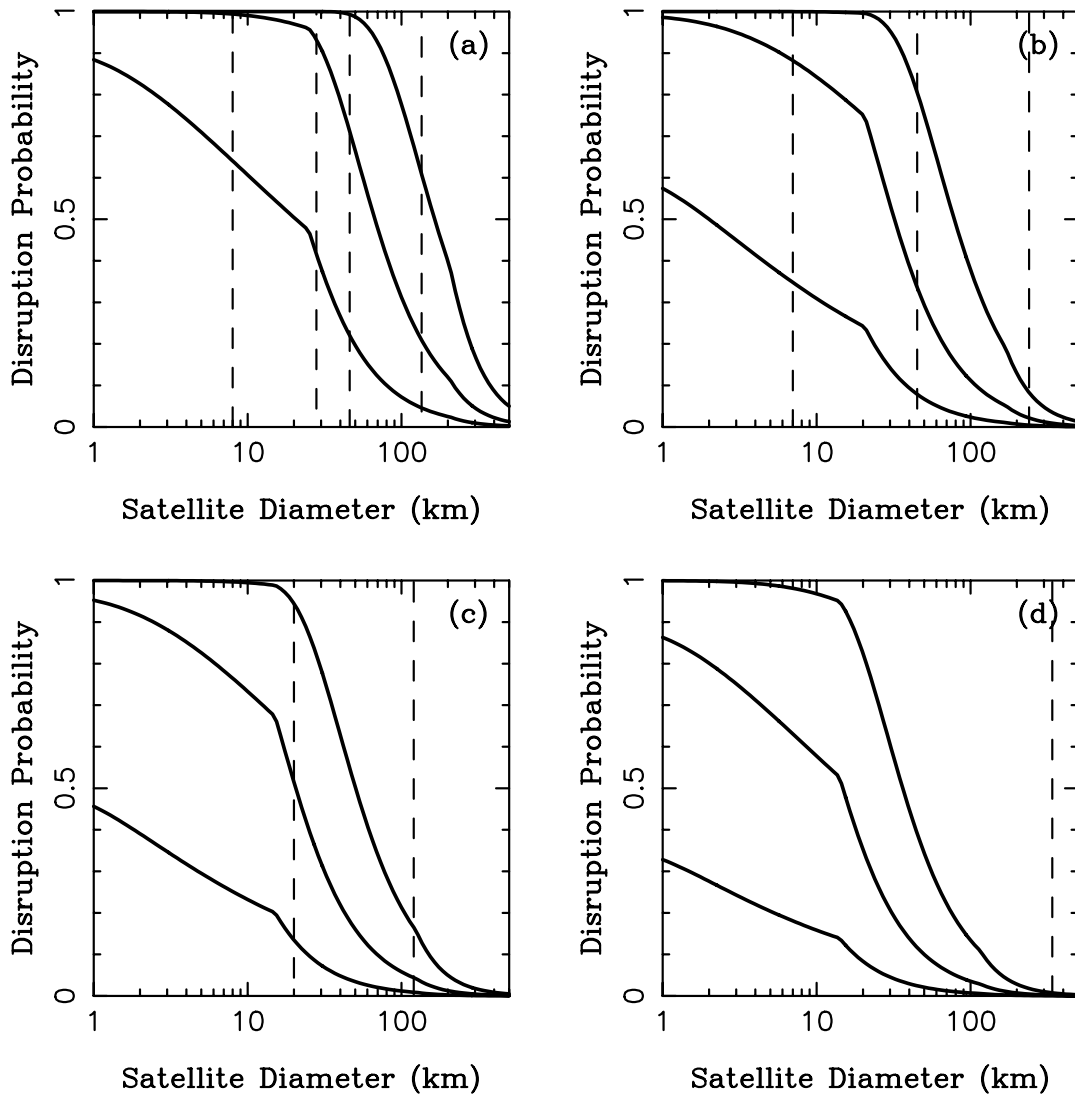


FIG. 5.—Same as Fig. 4, but for $N_B(>d)$ (eq. [7])

an external planetesimal impactor is unlikely for even large M_{disk} and independent of whether we use the case A, B, or C distribution. We discuss this interesting case below. Themisto, a $D = 8$ km prograde irregular moon of Jupiter, does not seem to be related to the Himalia family. Its survival is more problematic and requires small M_{disk} , the case A distribution, or both. In general, the case A distribution poses weaker constraints on M_{disk} because $p(D) < 0.7$ at Jupiter for any D with $M_{\text{disk}} \lesssim 50 M_{\oplus}$ (Fig. 4a).

The constraints shown in Figures 4–6 for satellites of Jupiter are shown in a different way in Table 3. (We focus on the Jovian system because much smaller irregular moons have been discovered at Jupiter than around the other giant planets. Thus, Jovian satellites provide the strongest observational constraint.) We list the range of satellite diameters D_D (for case A) or the maximum diameter (cases B and C) for which disruption of a given moon is 50%, 95%, or 99% likely. Cases B and C constrain the mass of the protoplanetary disk to be less than $50 M_{\oplus}$ (and for case C, much less) at the time when the present-day irregular satellites formed. Jupiter has 20 known irregular moons with $D \leq 2$ km. It seems most unlikely that these are the surviving remnants of a population of 2000 irregular moons (assuming 99% were

destroyed).¹¹ Thus, we reject models in which $D_D(99\%) > 2$ km. This criterion implies that $M_{\text{disk}} < 27 M_{\oplus}$ for case B and $M_{\text{disk}} < 0.4 M_{\oplus}$ for case C. These correspond to upper limits of 1×10^{12} and 6×10^{10} planetesimals with $d > 1.5$ km at the time the irregular satellites formed. (By contrast, if the “scattered disk” of comets beyond Neptune is the source of the Jupiter-family comets [Duncan, Levison, & Dones 2004], the scattered disk must contain some 10^8 – 10^9 such planetesimals at present [Bottke et al. 2002.]) Thus, at the time the irregular satellites formed, the protoplanetary disk would have been depleted compared with the original disk, but much more populous than at present.

Phoebe ($D = 240$ km), Sycorax ($D = 120$ km), and Nereid ($D = 340$ km) outlast the phase of heavy bombardment by

¹¹ Because $\sim 50\%$ of the small irregular moons at Jupiter that we see today are members of the Carme and Ananke families, having 2000 or more defunct small irregular moons in total would mean that the Carme and Ananke families originally had ≥ 50 times more multikilometer members than they have today. Consequently, they would correspond to large-scale catastrophic collisions rather than to the smaller scale cratering impacts that we favor in this work. Although such catastrophic collisions cannot be ruled out, we believe that small-scale cratering impacts are a more straightforward interpretation of the current observational data.

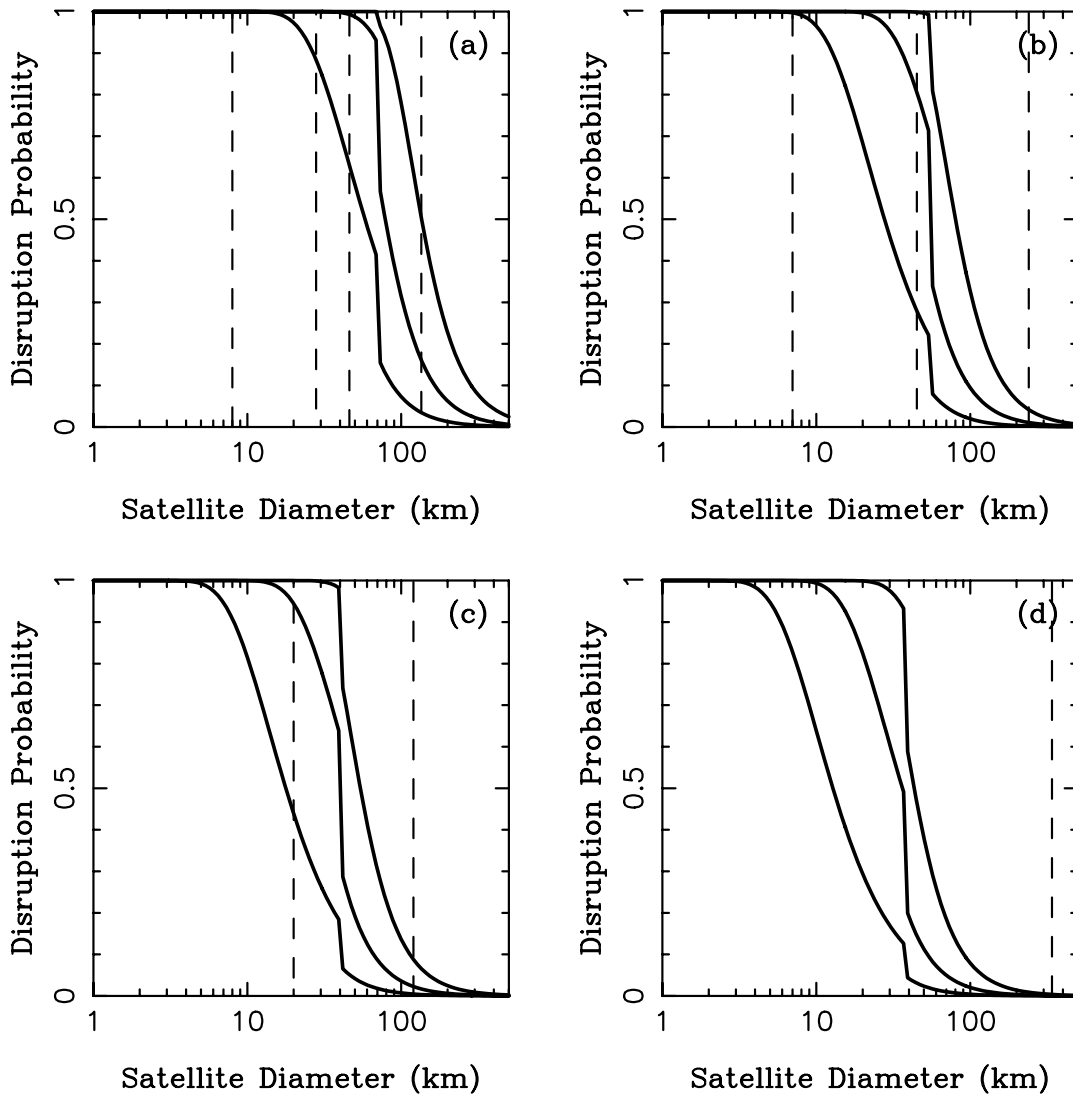


FIG. 6.—Same as Fig. 4, but for $N_C(>d)$ (eq. [8])

planetesimals for any plausible M_{disk} . Other known irregular satellites of Saturn and Uranus range in size from $D \sim 7$ to $D \sim 60$ km. With the case C distribution, these smaller satellites require small M_{disk} . In particular, $p(D) < 0.5$ for $D > 30$ km with $M_{\text{disk}} = 10 M_{\oplus}$ at Saturn (Fig. 6b). Thus, survival of many $D \lesssim 30$ km irregular moons at Saturn is problematic unless $M_{\text{disk}} \ll 10 M_{\oplus}$, or the observed moons represent only a small fraction of the original population. Cases A and B (Figs. 4 and 5) place weaker constraints on M_{disk} .

Some time after their captures occurred, some of the moons suffered energetic (but probably subcatastrophic) collisions (e.g., Ananke and Carme; § 2). The tight clustering of orbits of the Ananke and Carme family members suggests that the circumplanetary gas envelope had already dissipated at the time when these collisions occurred. Otherwise, the size-dependent aerodynamic gas drag would disperse these clusters and sort them according to the moons' diameters, which is not observed (see, e.g., Gladman et al. 2001a). Using equation (19) and typical impact speeds and ejecta mass (§ 2) for the Ananke and Carme families, we estimate the required size for a planetesimal impactor d . Using this size, the SFD of impactors, and impact probabilities, we then determine the

minimum required M_{disk} that yields cratering impacts of diameter d planetesimals on Ananke and Carme.

With a 6.7 km s^{-1} impact speed (Table 2) for an impact on Ananke and equation (19), we find that a planetesimal impactor with $d \sim 0.53$ km and 1 g cm^{-3} bulk density would excavate and disperse enough material to produce the observed members of the Ananke family. Similarly, a $d \sim 0.59$ km impactor is needed in order to create the Carme family if it collides with Carme at $\sim 6.6 \text{ km s}^{-1}$. Both these collisions are subcatastrophic, because $M_{\text{LF}}/M_{\text{PB}} \sim 0.96$ and 0.99 , where M_{LF} and M_{PB} are the masses of the largest fragment and the parent body, respectively. The specific energies of these impacts are 1.5×10^6 and $4.5 \times 10^5 \text{ ergs g}^{-1}$, or only $\sim 2.3\%$ and $\sim 0.4\%$ of Q_D^* defined by equation (18). We calculate that to have a $\geq 50\%$ probability that an impact of this energy or greater occurred on Ananke, $M_{\text{disk}} \geq 8 M_{\oplus}$ with case A, $M_{\text{disk}} \geq 1.7 M_{\oplus}$ with case B, and $M_{\text{disk}} \geq 0.2 M_{\oplus}$ with case C. For Carme, we find $M_{\text{disk}} \geq 3.3 M_{\oplus}$ with case A, $M_{\text{disk}} \geq 0.7 M_{\oplus}$ with case B, and $M_{\text{disk}} \geq 0.1 M_{\oplus}$ with case C. The required values of M_{disk} are very sensitive to the assumed SFD of planetesimals because our cases A, B, and C have very different power indices at subkilometer impactor sizes. Nevertheless, all calculated values for M_{disk} are plausible,

TABLE 3
CONSTRAINTS ON THE MASS OF THE PLANETESIMAL DISK FROM THE
KNOWN SIZES OF THE JOVIAN IRREGULAR SATELLITES

M_{disk}	$D_D(50\%)$	$D_D(95\%)$	$D_D(99\%)$
Case A:			
10.....
50.....	9–69
200.....	1–169	10–66	21–33
Case B:			
10.....	21
50.....	67	26	10
200.....	164	64	48
Case C:			
10.....	55	22	17
50.....	79	64	48
200.....	136	76	70

NOTES.—For three assumed size distributions (cases A, B, and C) and total heliocentric disk masses (10, 50, and 200 M_{\oplus}), we list the range of Jovian satellite diameters (D_D) such that 50%, 95%, and 99% of the satellites would have been catastrophically disrupted and dispersed. The case A size distribution has the fewest kilometer-sized (and smaller) impactors for a given disk mass, while case C has the most such impactors, so that satellite destruction probabilities are larger for case C than for the other cases. For example, in case A with a 10 M_{\oplus} disk, all satellites with diameters $D > 1$ km have better than a 50% chance of survival. In case A with a 200 M_{\oplus} disk, satellites with diameters between 10 and 66 km have at least a 95% chance of being destroyed, while both smaller and larger satellites are more likely to survive (see Fig. 4). For cases B and C, the probability of destruction is a monotonically decreasing function of satellite diameter, so we only list one number, the upper limit on D . For example, for case C and a 10 M_{\oplus} disk, satellites with $D \leq 17$ km have a 99% chance of being catastrophically disrupted. We also indicate with boldface the cases that are inconsistent with the known sizes of the Jovian irregular satellites.

making it conceivable that the Ananke and Carme families were, indeed, produced by impacts of subkilometer planetesimals during early epochs. To summarize, to form the Ananke and Carme families by this mechanism, we require an M_{disk} of the contemporary disk that is only a small fraction of the mass of solids initially present (Hayashi 1981; Hahn & Malhotra 1999).

Another interesting and related issue is the provenance of the prograde Himalia group at Jupiter. We estimate from the observed members of the Himalia family that the prograde group progenitor was a body ~ 150 km across. If so, $M_{\text{IF}}/M_{\text{PB}} \sim 0.78$. This ratio is smaller and requires a larger scale impact than that needed to explain the Ananke and Carme families. Using equation (19) and a 7.7 km s^{-1} impact speed (Table 2), we calculate that a $d \sim 13$ km planetesimal must have impacted the prograde group progenitor body. The specific energy of this impact is $2.1 \times 10^8 \text{ ergs g}^{-1}$, or about 40% of Q_D^* (eq. [18]), which is in perfect agreement with the scaling for sub-catastrophic collisions given by Benz & Asphaug (1999; their eq. [8]).

We calculate that to have a $\geq 50\%$ probability that an impact of this energy occurred on the prograde group progenitor, $M_{\text{disk}} \geq 70 M_{\oplus}$ for any of our three SFDs. These values of M_{disk} may be too large (Hahn & Malhotra 1999; Beugé et al. 2002) unless Himalia was captured very early. In that case, it probably would have been swallowed by Jupiter as a result of gas drag or density wave torques. We thus believe that the Himalia group probably did not form by an impact of a stray planetesimal. Instead, we speculate that

the progenitor of the Himalia family was hit and disrupted more recently by an impact of another irregular satellite of Jupiter. Nesvorný et al. (2003a) found that the expected number of impacts between Himalia and Elara is ≈ 1.5 per 4.5 Gyr and that such a collision would be catastrophic. It is difficult to characterize the disruption history of Himalia more precisely, because satellites in the Himalia group probably suffered other collisions between themselves since their formation (Nesvorný et al. 2003a).

The Phoebe group at Saturn (Gladman et al. 2001a) poses another intriguing problem that requires explanation. If this group formed by a collision of Phoebe with a stray planetesimal, we calculate that a $d \sim 3$ km planetesimal impacting at 5.1 km s^{-1} (Table 2) and excavating a ~ 40 km diameter crater on Phoebe's surface can best explain it. It is likely that such an event would occur (i.e., with over 50% probability) if $M_{\text{disk}} \geq 0.2\text{--}1.4 M_{\oplus}$ at the time when Phoebe was captured, with the exact value depending on the detailed profile of the planetesimals' SFD. It is thus statistically plausible that the Phoebe group was created by such an event. What is less well understood is the unusually large δV ($100\text{--}400 \text{ m s}^{-1}$) calculated for the Phoebe group members from the Gauss equations (Nesvorný et al. 2003a). Even more striking is the fact that the outermost satellites of this group do not intersect the orbit of Phoebe (Čuk & Burns 2004). It is possible that some yet-to-be-identified mechanism dispersed fragments of the Phoebe group after its formation, or that its members have other (possibly unrelated) origins.

9. CONCLUSION

We proposed that the Ananke and Carme families of irregular satellites at Jupiter formed during early epochs when Ananke and Carme were cratered by impacts of stray planetesimals from the residual protoplanetary disk. Conversely, we found that formation of the Himalia group by the same mechanism is unlikely unless a massive residual planetesimal disk was still present when the parent body of the Himalia group was captured. We speculate that the Himalia family formed more recently by a collision of its progenitor with another irregular satellite of Jupiter.

We placed constraints on the mass of the residual disk (1) when satellites were captured, and (2) when the Ananke and Carme families formed. These values depend sensitively on the assumed size-frequency distribution of planetesimals. For example, we require $M_{\text{disk}} \lesssim 10 M_{\oplus}$ to guarantee survival of the retrograde irregular satellites at Jupiter with $28 \text{ km} \lesssim D \lesssim 60 \text{ km}$ diameters (Ananke, Carme, Pasiphae, and Sinope), if our case C distribution applies. Similarly, we estimated that $M_{\text{disk}} \geq 0.1\text{--}8 M_{\oplus}$ is required to produce the Ananke and Carme families by cratering impacts of planetesimals on Ananke and Carme.

Unfortunately, we cannot draw stronger constraints on M_{disk} because of the uncertainty caused by the poorly known profile of the size-frequency distribution of planetesimals. By using three distributions, we made an effort to span a realistic range of SFDs. It may be that the case C distribution is more realistic for the primordial planetesimal disk and that the case A and B distributions, which are more characteristic for ecliptic comets, have resulted from later collisional grinding in the Kuiper belt. We do not know. Hopefully, future studies of these issues will help us to select a specific SFD and calibrate constraints generated by this work on M_{disk} to this distribution.

We would like to thank the referee, Derek Richardson, for his helpful comments. This paper is based upon work supported by the National Science Foundation under grant AST 00-74163.

APPENDIX

THE JACOBI CONSTANT IN PLANETOCENTRIC ELEMENTS

We consider a circular restricted three-body system consisting of the Sun, a planet, and a planetesimal with infinitesimal mass in heliocentric orbit. In this system, the Jacobi constant C is an integral of the motion. Although this function is usually written in the Cartesian coordinates of a rotating reference frame, we can also express C in terms of the coordinates of the fixed nonrotating system (Brouwer & Clemence 1961) as

$$C = \frac{GM_{\odot}}{r_h} + \frac{GM_0}{r_p} + n_0(x_h\dot{y}_h - y_h\dot{x}_h) - \frac{V_h^2}{2}, \quad (\text{A1})$$

where G is the gravitational constant, M_{\odot} and M_0 are the solar and planetary masses, n_0 is the mean motion of the planet, (x_h, y_h, z_h) are the heliocentric Cartesian coordinates of the planetesimal, and V_h is its heliocentric speed. Finally, r_h and r_p are respectively the heliocentric and planetocentric distances of the planetesimal.

Denoting by (x_0, y_0, z_0) the heliocentric coordinates of the planet, we obtain the planetocentric coordinates of the planetesimal (x_p, y_p, z_p) from its heliocentric coordinates (x_h, y_h, z_h) as

$$x_p = x_h - x_0, \quad y_p = y_h - y_0, \quad z_p = z_h - z_0. \quad (\text{A2})$$

Expressions for the velocities are analogous. Assuming $\dot{z}_0 = 0$, we can write

$$V_h^2 = V_p^2 + V_0^2 + 2(\dot{x}_p\dot{x}_0 + \dot{y}_p\dot{y}_0), \quad (\text{A3})$$

where V_p and V_0 are the planetocentric speed of a planetesimal and the heliocentric speed of the planet, respectively. Similarly, we have

$$x_h\dot{y}_h - y_h\dot{x}_h = (x_p\dot{y}_p - y_p\dot{x}_p) + (x_0\dot{y}_0 - y_0\dot{x}_0) + (x_p\dot{y}_0 - y_0\dot{x}_p) + (x_0\dot{y}_p - y_p\dot{x}_0). \quad (\text{A4})$$

Because the orbit of the planet is assumed to be circular,

$$\begin{aligned} x_0 &= a_0 \cos \lambda_0, & \dot{x}_0 &= -a_0 n_0 \sin \lambda_0, \\ y_0 &= a_0 \sin \lambda_0, & \dot{y}_0 &= a_0 n_0 \cos \lambda_0, \end{aligned} \quad (\text{A5})$$

where λ_0 is the mean longitude of the planet. Similarly, we can express the planetocentric coordinates of the planetesimal as

$$\begin{aligned} x_p &= r_p \cos(f + \varpi), & y_p &= r_p \sin(f + \varpi), \\ \dot{x}_p &= \dot{r}_p \cos(f + \varpi) - r_p \dot{f} \sin(f + \varpi), \\ \dot{y}_p &= \dot{r}_p \sin(f + \varpi) + r_p \dot{f} \cos(f + \varpi), \end{aligned} \quad (\text{A6})$$

where this is written in terms of the *planetocentric* orbital elements: f is the true anomaly and ϖ is the longitude of the pericenter.

In the following, we will write C as a function of planetocentric orbital elements at pericenter. We require that

$$f = 0, \quad r_p = q, \quad \dot{r} = 0. \quad (\text{A7})$$

Introducing these expressions into equations (A3) and (A4), we obtain

$$\begin{aligned} x_h\dot{y}_h - y_h\dot{x}_h &= (x_p\dot{y}_p - y_p\dot{x}_p) + (x_0\dot{y}_0 - y_0\dot{x}_0) \\ &\quad + r_p a_0 (n_0 + \dot{f}) \cos(\varpi - \lambda_0), \\ V_h^2 &= V_p^2 + V_0^2 + 2r_p a_0 n_0 \dot{f} \cos(\varpi - \lambda_0). \end{aligned} \quad (\text{A8})$$

Before introducing these new expressions into C , we can simplify them further. For example, we can use the following relationships:

$$\begin{aligned} x_p\dot{y}_p - y_p\dot{x}_p &= h \cos i, \\ x_0\dot{y}_0 - y_0\dot{x}_0 &= [G(M_{\odot} + M_0)a_0]^{1/2}, \\ V_0^2 &= G(M_{\odot} + M_0)/a_0, \\ r_s^2 &= q^2 + a_0^2 - 2qa_0 \cos(\varpi - \lambda_0), \end{aligned} \quad (\text{A9})$$

where h is the planetocentric angular momentum per unit mass of the planetesimal. Similarly, at pericenter, we have that

$$\dot{f} = h/q^2, \quad V_p = h/q, \quad (\text{A10})$$

which allow us to write the angular and linear velocities in terms of the angular momentum.

Finally, introducing all these expressions into the equations for C and grouping terms in powers of h , we obtain

$$C = c_0 + c_1 h + c_2 h^2, \quad (\text{A11})$$

where the functions c_i are given in equations (11)–(12). These expressions constitute a precise relationship between the planetocentric elements of a planetesimal at pericenter and C .

REFERENCES

- Beaugé, C., Roig, F., & Nesvorný, D. 2002, *Icarus*, 158, 483
Benz, W., & Asphaug, E. 1999, *Icarus*, 142, 5
Bierhaus, E. B., Chapman, C. R., & Merline, W. J. 2003, *BAAS*, 35, Div. Planet. Sci. abstr. No. 6.08
Bierhaus, E. B., Chapman, C. R., Merline, W. J., Brooks, S. M., & Asphaug, E. 2001, *Icarus*, 153, 264
Bottke, W. F., & Greenberg, R. 1993, *Geophys. Res. Lett.*, 20, 879
Bottke, W. F., Morbidelli, A., Jedicke, R., Petit, J.-M., Levison, H. F., Michel, P., & Metcalfe, T. S. 2002, *Icarus*, 156, 399
Brouwer, D., & Clemence, G. M. 1961, *Methods of Celestial Mechanics* (New York: Academic)
Brown, M. E. 2000, *AJ*, 119, 977
Burns, J. A. 1986, in *Satellites*, ed. J. A. Burns & M. S. Matthews (Tucson: Univ. Arizona Press), 1
Canup, R. M., & Ward, W. R. 2002, *AJ*, 124, 3404
Colombo, G., & Franklin, F. A. 1971, *Icarus*, 15, 186
Croft, S. K., Kargel, J. S., Kirk, R. L., Moore, J. M., Schenk, P. M., & Strom, R. G. 1995, in *Neptune and Triton*, ed. D. P. Cruikshank (Tucson: Univ. Arizona Press), 879
Čuk, M., & Burns, J. A. 2004, *Icarus*, 167, 369
Dohnanyi, J. S. 1972, *Icarus*, 17, 1
Duncan, M. J., Levison, H. F., & Dones, L. 2004, in *Comets II*, ed. M. Festou, H. U. Keller, & H. A. Weaver (Tucson: Univ. Arizona Press), in press
Gladman, B., et al. 2001a, *Nature*, 412, 163
Gladman, B., Kavelaars, J. J., Holman, M., Petit, J.-M., Scholl, H., Nicholson, P., & Burns, J. A. 2000, *Icarus*, 147, 320 (erratum 148, 320)
Gladman, B., Kavelaars, J. J., Petit, J.-M., Morbidelli, A., Holman, M. J., & Loredó, T. 2001b, *AJ*, 122, 1051
Gladman, B. J., Nicholson, P. D., Burns, J. A., Kavelaars, J. J., Marsden, B. G., Williams, G. V., & Offutt, W. B. 1998, *Nature*, 392, 897

- Grav, T., Holman, M. J., Gladman, B. J., & Aksnes, K. 2003, *Icarus*, 166, 33
- Hahn, J. M., & Malhotra, R. 1999, *AJ*, 117, 3041
- Hayashi, C. 1981, *Prog. Theor. Phys. Suppl.*, 70, 35
- Hayashi, C., Nakazawa, K., & Nakagawa, Y. 1985, *Protostars and Planets II*, ed. D. C. Black & M. S. Matthews (Tucson: Univ. Arizona Press), 1100
- Hirayama, K. 1918, *AJ*, 31, 185
- Holman, M., Kavelaars, J., Grav, T., Fraser, W., & Milisavljevic, D. 2003, *IAU Circ.* 8047
- Kary, D. M., & Dones, L. 1996, *Icarus*, 121, 207
- Kenyon, S. J. 2002, *PASP*, 114, 265
- Kenyon, S. J., & Luu, J. X. 1998, *AJ*, 115, 2136
- Kessler, D. J. 1981, *Icarus*, 48, 39
- Kuiper, G. P. 1949, *PASP*, 61, 175
- Luu, J. 1991, *AJ*, 102, 1213
- Manley, S. P., Migliorini, F., & Bailey, M. E. 1998, *A&AS*, 133, 437
- Michel, P., Benz, W., Tanga, P., & Richardson, D. C. 2001, *Science*, 294, 1696
- Mosqueira, I., & Estrada, P. R. 2003a, *Icarus*, 163, 198
- . 2003b, *Icarus*, 163, 232
- Nesvorný, D., Alvarillos, J. L. A., Dones, L., & Levison, H. F. 2003a, *AJ*, 126, 398
- Nesvorný, D., Bottke, W. F., Jr., Dones, L., & Levison, H. F. 2002, *Nature*, 417, 720
- Nesvorný, D., Bottke, W. F., Levison, H. F., & Dones, L. 2003b, *ApJ*, 591, 486
- Nesvorný, D., & Dones, L. 2002, *Icarus*, 160, 271
- Öpik, E. J. 1951, *Proc. R. Irish Acad. A*, 54, 165
- Pollack, J. B., Burns, J. A., & Tauber, M. E. 1979, *Icarus*, 37, 587
- Porco, C. C., et al. 2003, *Science*, 299, 1541
- Rettig, T. W., Walsh, K., & Consolmagno, G. 2001, *Icarus*, 154, 313
- Richardson, D. C., Leinhardt, Z. M., Melosh, H. J., Bottke, W. F., Jr., & Asphaug, E. 2002, in *Asteroids III*, ed. W. F. Bottke, A. Cellino, P. Paolicchi, & R. P. Binzel (Tucson: Univ. Arizona Press), 501
- Schenk, P. M., Chapman, C., Moore, J., & Zahnle, K. 2004, in *Jupiter*, ed. F. Bagenal, T. Dowling, & W. McKinnon (Cambridge: Cambridge Univ. Press), in press
- Schmidt, R. M., & Housen, K. R. 1987, *Int. J. Impact Eng.*, 5, 543
- Sheppard, S. S., & Jewitt, D. C. 2003, *Nature*, 423, 261
- Shoemaker, E. M., & Wolfe, R. F. 1982, in *Satellites of Jupiter*, ed. D. Morrison (Tucson: Univ. Arizona Press), 277
- Stern, S. A. 1995, *AJ*, 110, 856
- Stern, S. A., & McKinnon, W. B. 2000, *AJ*, 119, 945
- Sykes, M. V., Nelson, B., Cutri, R. M., Kirkpatrick, D. J., Hurt, R., & Skrutskie, M. F. 2000, *Icarus*, 143, 371
- Thomas, P., Veverka, J., & Helfenstein, P. 1991, *J. Geophys. Res.*, 96, 19253
- Trujillo, C. A., Jewitt, D. C., & Luu, J. X. 2001, *AJ*, 122, 457
- Zahnle, K., Dones, L., & Levison, H. F. 1998, *Icarus*, 136, 202
- Zahnle, K., Schenk, P., Levison, H., & Dones, L. 2003, *Icarus*, 163, 263
- Zahnle, K., Schenk, P., Sobieszczyk, S., Dones, L., & Levison, H. F. 2001, *Icarus*, 153, 111
- Zappalà, V., Cellino, A., Farinella, P., & Milani, A. 1994, *AJ*, 107, 772